Understanding and improving photo-control of ion channels in nociceptors with azobenzene photo-switches

Alexandre Mourot, Christian Herold, Michael A Kienzler, Richard H Kramer

Understanding and improving photo-control of ion channels in nociceptors with azobenzene photoswitches

Alexandre Mourot[1*], Christian Herold[2,3*], Michael A. Kienzler[4] and Richard H. Kramer[2]

Affiliations:
1: Sorbonne Universités, UPMC Univ Paris 06, INSERM, CNRS, Neuroscience Paris Seine - Institut de Biologie Paris Seine (NPS - IBPS), 75005 Paris, France
2: Department of Molecular and Cell Biology, University of California Berkeley, Berkeley, CA 94720, USA
3: Biophysics Graduate Group, University of California Berkeley, Berkeley, CA 94720, USA
4: Department of Chemistry, University of Maine, Orono, ME 04469, USA

* These authors contributed equally.

Correspondence to: almourot@gmail.com or rhkramer@berkeley.edu

Abstract:

- Background and Purpose: We previously developed a photoisomerizable local anaesthetic, named QAQ, to gain rapid, optical control over pain signaling without involving genetic modification. In darkness or in green light, *trans*-QAQ blocks voltage-gated K^+ and Na^+ channels and silences action potentials in pain-sensing neurons. Upon photoisomerization to *cis* with near UV light, QAQ blockade is rapidly relieved and neuronal activity is restored. However, the molecular mechanism of *cis* and *trans* QAQ blockade is not known. Moreover, the absorption spectrum of QAQ requires UV light for photo-control, precluding use deep inside neural tissue.

- Experimental Approach: We have used electrophysiology and molecular modelling to characterize the binding of *cis* and *trans* QAQ to voltage-gated K^+ channels, and we have developed QENAQ, a red-shifted QAQ derivative that is controlled with visible light.

- Key Results: *Trans* QAQ blocked current through Shaker K^+ channel with a 6-fold greater potency than *cis* QAQ. Both isomers were use-dependent, open channel blockers that bind from the cytoplasmic side, but only *trans* QAQ block was slightly voltage dependent. QENAQ also blocked native K^+ and Na^+ channels preferentially in the *trans* state. QENAQ was photoisomerized to *cis* with blue light, and spontaneously reverted to *trans* within seconds in darkness, enabling rapid photo-control of action potentials in sensory neurons.

- Conclusion and Implications. Light-switchable local anaesthetics provide a means to non-invasively photo-control pain signalling with high selectivity and fast kinetics. Understanding the mode of action of QAQ and related compounds will help in the design of drugs with improved photo-pharmacological properties.

Non-approved abbreviations: AAQ: acrylamide - azobenzene - quaternary ammonium; ACSF: artificial cerebrospinal fluid solution; BzAQ: Benzoyl – azobenzene - quaternary ammonium; CAP: Compound Action Potential ; DRG: dorsal root ganglion; Ip: peak current; Iss: steady-state current; MEA: multi electrode array; ORI: Oocyte Ringer solution; P2X7: ATP-gated ion channel 7; PI: photoswitching index; QAQ: quaternary ammonium - azobenzene - quaternary ammonium; QENAQ: quaternary ammonium - ethylamine - azobenzene - quaternary ammonium; Shaker-IR: Shaker-inactivation removed; TEA: tetra-ethyl ammonium; TG: trigeminal ganglion; TRPV1: transient receptor potential vanilloid receptor 1

Plain Language Summary:
Drugs that can be rapidly turned on and off with light offer the possibility to solve the issues of toxicity and side effects of classical pharmacotherapies. Here we have characterized and tuned the photo-pharmacological properties of a light-sensitive local anaesthetic, and we achieved optical control of pain signalling with blue light, without genetic engineering.

- Introduction

Local anaesthetics decrease pain sensation by silencing the firing of nociceptor neurons. However, local anaesthetics can also silence other sensory and motor neurons, leading to serious side effects, especially when the drugs are applied for an extended period of time. We have been developing light-sensitive local anaesthetics that can be controlled with spatio-temporal precision, and which act specifically on nociceptors, avoiding side effects.

Optopharmacology (or photopharmacology) refers to the use of photosensitive drugs that change structure upon irradiation with light (Kramer et al., 2013; Velema et al., 2014; Lerch et al., 2016). The aim is to establish precise, optical control over the activity, the kinetics, and the site of action of a bioactive compound. Optopharmacological agents are rationally designed to incorporate in their structure a chemical photoswitch, which confers to the drug its photosensitivity. Azobenzene is a commonly used photoswitch, owing to the considerable geometrical difference between its bent, *cis* and straight, *trans* configuration (Fehrentz et al., 2011; Szymański et al., 2013). Upon photoisomerization, azobenzene-containing drugs change shape, affecting their binding to target receptors, and hence their biological activity. Azobenzene can be rapidly switched back and forth between their two isomers to enable control over receptors with high temporal precision (ms). Light can be delivered with high spatial precision to restrict the action of azobenzene-containing drugs to a tightly localized region in biological tissue. Finally, the wavelength and/or intensity of incident light can be adjusted to change the ratio between *trans* and *cis* isomers, altering the effective concentration of the active form of the compound interacting with the receptor.

We previously developed a series of photoswitchable blockers for voltage-gated K^+ channels, named XAQs (Banghart et al., 2009; Mourot et al., 2011; 2012; 2013a; 2013b). XAQs possess a quaternary ammonium group (Q), which binds to the cytoplasmic tetra-ethyl ammonium (TEA) binding site on K^+ channels, a central azobenzene photoswitch (A), and a terminal aliphatic chain of variable structure (X). XAQs are permanently charged, yet most are sufficiently hydrophobic to passively cross the membrane bilayer and reach the cytoplasmic lumen on K^+ channels (Banghart et al., 2009). They have been used to optically control action potential firing in dissociated neurons (Banghart et al., 2009), brain slices (Mourot et al., 2011) and in the retina for restoring visual responses in blind mice (Polosukhina et al., 2012; Tochitsky et al., 2014; 2016). One of these photoswitchable blockers, QAQ (quaternary ammonium - azobenzene - quaternary ammonium, Fig. 1A) has two important features that distinguish it from other XAQs: 1) it contains two permanently charged quaternary ammonium groups, and therefore cannot passively cross the membrane bilayer; and 2) it is not selective for voltage-gated K^+ channels but also photosensitizes voltage-gated Na^+ and Ca^{2+} channels (Mourot et al., 2012). QAQ can be loaded into neurons by two means: either artificially using the patch pipette, or "naturally" by passing through open ion channels with large pores that are endogenous to some neurons, such as the P2X7 receptor and the TRPV1 channel. Once inside neurons, *trans* QAQ blocks many voltage-gated ion channels and silences neuronal activity in the dark, while illumination with violet light isomerises the molecule to *cis*, relieving blockade and restoring excitability.

QAQ is structurally and functionally similar to the membrane-impermeant, lidocaine derivative QX-314 (Fig. 1B, (Strichartz, 1973)), with the additional benefit of being photo-controllable. Lidocaine (Fig. 1C) is a potent local anaesthetic that prevents signal propagation to the brain, by blocking voltage-gated Na^+ and other ion channels (Fozzard et al., 2011). Because lidocaine is membrane permeant when deprotonated, however, it silences not only

pain-sensing neurons but also other sensory and motor neurons. In contrast, both QX-314 and QAQ fail to block Na$^+$ channels when applied outside cells, but are potent blockers once introduced inside cells. In a clever experimental design, Binshtok et al. achieved nociceptive-selective analgesia using QX-314 (Binshtok et al., 2007). They found that this molecule could enter nociceptors selectively by passing through the pore of noxious-heat sensitive TRPV1 channels, which are highly expressed in nociceptors but scarcely present in other neuronal cell types (Binshtok et al., 2007). Similarly, we found that QAQ could selectively silence pain-sensing neurons, while leaving other sensory modalities unaffected. But unlike QX-314 which produces long-lasting analgesia (Binshtok et al., 2009), the effect of QAQ can be reversed within seconds using flashes of near-UV light (Mourot et al., 2012). QAQ can therefore function as a targeted, light-tunable local anaesthetic, both *ex* and *in vivo*.

However, how the two isomers of QAQ block ion channels is unclear. In addition, the short wavelength of light necessary to effectively switch QAQ to *cis* can be cell damaging, and poorly penetrates intact tissue. Therefore, we sought a mechanistic understanding of QAQ action on ion channels, to inform chemical modifications that could improve photo-control in neural tissue. We probed *cis* and *trans* QAQ binding using electrophysiology and molecular modelling. We chose the Shaker K$^+$ channel, a prototypical voltage-gated ion channel with well-understood biophysical properties, as a model system to study QAQ-ion channel interactions. Having established how QAQ interacts with Shaker K$^+$ channels, we have designed a red-shifted version of QAQ (QENAQ) that photoisomerizes to *cis* using blue light and reverts back to *trans* within seconds in darkness. We further show that QENAQ can be used to optically control action potential firing in intact dorsal root ganglia. Insights from QAQ and QENAQ will inspire the design of related compounds with tuned properties, expanding this group of optical tools for neuronal control, both for gaining scientific insights and as potential therapeutic agents.

- Methods

Synthesis of QAQ and QENAQ
QAQ was synthesized as described in (Mourot et al., 2012). QENAQ was synthesized as described in Scheme 1. Reactions were carried out under nitrogen atmosphere and magnetically stirred in oven-dried glassware.

(E)-2-((4-((4-aminophenyl)diazenyl)phenyl)(ethyl)amino)-N,N,N-triethylethan-1-aminium (B): 4-((4-aminophenyl)diazenyl)-N-(2-bromoethyl)-N-ethylaniline (A, 63 mg, 0.182 mmol (Kienzler et al., 2013)) was transferred to a heavy-walled pressure vessel and dissolved in ethanol (4 mL), dichloromethane (0.5 mL), and triethylamine (0.2 mL). The mixture was sparged with nitrogen gas and the flask was sealed and then heated to 80 °C for 5 days. The reaction mixture was concentrated in vacuo and the residue purified by reverse phase (C-18 silica gel) flash column chromatography (0% to 40% methanol in 0.1% aqueous formic acid) to yield 26.5 mg (40%) of B as a red solid. ^{1}H NMR (500 MHz, Methanol-d_4) δ 7.77 (d, J = 8.6 Hz, 2H), 7.63 (d, J = 8.5 Hz, 2H), 6.90 (d, J = 8.8 Hz, 2H), 6.74 (d, J = 8.6 Hz, 2H), 3.85 (t, J = 7.7 Hz, 2H), 3.54 (q, J = 6.9 Hz, 2H), 3.44 (m, 8H), 1.35 (t, J = 7.2 Hz, 9H), 1.23 (t, J = 6.9 Hz, 3H); HRMS (ESI+) m/z calcd for $C_{22}H_{34}N_5$ [M]$^+$: 368.2808, found 368.2809.

QENAQ: Freshly prepared 2-chloro-N,N,N-triethyl-2-oxoethan-1-aminium (**C**, 150 mg, 0.842 mmol (Banghart et al., 2009)) dissolved in acetonitrile (5 mL) was slowly added to a stirred flask containing (E)-2-((4-((4-aminophenyl)diazenyl)phenyl)(ethyl)amino)-N,N,N-triethylethan-1-aminium (**B**, 18.5 mg, 0.050 mmol) dissolved in acetonitrile (5 mL) and diisopropylethylamine (0.2 mL), all of which was cooled to 0 °C in an ice bath. The reaction

was stirred and allowed to warm to room temperature overnight. The reaction mixture was concentrated in vacuo and the residue purified by reverse phase (C-18 silica gel) flash column chromatography (0% to 20% methanol in 0.1% aqueous formic acid) to yield 14 mg (55%) of QENAQ as a red solid. ^{1}H NMR (600 MHz, Methanol-d_4) δ 7.88 (d, J = 9.1 Hz, 2H), 7.84 (d, J = 8.8 Hz, 2H), 7.77 (d, J = 8.8 Hz, 2H), 6.93 (d, J = 9.2 Hz, 2H), 4.22 (s, 2H), 3.90 (s, 2H), 3.69 (q, J = 7.3 Hz, 6H), 3.58 (q, J = 7.1 Hz, 2H), 3.50 – 3.42 (m, 8H), 1.40 (t, J = 7.2 Hz, 9H), 1.37 (t, J = 7.2 Hz, 9H), 1.26 (t, J = 7.0 Hz, 3H); ^{13}C NMR (151 MHz, Methanol-d_4) δ 163.14, 151.22, 150.86, 145.75, 140.33, 126.20, 124.07, 121.58, 113.65, 55.88, 55.85, 54.47, 49.57, 46.83, 44.03, 12.45, 7.99, 7.90; (ESI+) m/z calcd for $C_{30}H_{50}O_1N_6$ [M]$^{2+}$: 255.2021, found 255.2018.

UV/Vis spectra were measured at room temperature using a SmartSpec Plus photometer (Bio-Rad, USA).

Compliance with requirements for studies using animals

Male wild type mice (C57BL/6J strain, Jackson Laboratory) age 0-6 months were used in all experiments. All animal procedures were approved by the UC Berkeley Institutional Animal Care and Use Committee and were conducted in accordance with the NIH Guide for the Care and Use of Laboratory Animals. Animal studies are reported in compliance with the ARRIVE guidelines (McGrath and Lilley, 2015).

Expression of ion channel proteins in *Xenopus laevis* oocytes

Oocytes of maturation stage I to IV from *Xenopus leavis* frogs were surgically removed from female adults by laparotomy. Frogs were housed in a facility approved by OLAC of UC Berkeley. The animals were anesthetized by tricaine methane-sulfonate (MS-222, Western Chemical, USA) at neutral pH and individual frogs were used up to 6 times to harvest eggs. Removed oocytes were pre-digested with 1-2 mg/ml collagenase (Sigma, USA) to support defolliculation and connective membranes were manually removed. Oocytes with intact vitelline membranes were kept at 16°C in Oocyte Ringer solution (ORI, in mM: 96 NaCl, 2 KCl, 1 MgCl$_2$, 1.8 CaCl$_2$, 5 4-(2-hydroxyethyl)-1-piperazineethanesulfonic acid (HEPES), adjusted to pH 7.4 with NaOH). Shaker-IR (inactivation removed) expression was accomplished by injection of mRNA constructs which were synthesized from linearized DNA plasmids (mMessage mMachine T7 kit, Applied Biosystems, USA) containing Shaker-IR and a T7 site as previously described (Smart and Krishek, 1995). RNA injection took place 12 to 48 hours after oocyte harvest with a Nanoinject II microinjector (Drummond Scientific, USA) and injected oocytes were stored in ORI for 2-3 days at 16°C before recording, ORI buffer was replaced daily. Injection pipettes were pulled from borosillicate capillaries (Microcaps: inner diameter 0.70 mm, outer diameter 0.97 mm, Drummond Scientific, USA) with a micropipette puller (P-97, Sutter Instruments, USA). Tips were broken over a tissue cloth to have an approximate tip diameter of 15 μm, backfilled with colored mineral oil and loaded with RNA solution. RNA was diluted in ORI to a final concentration of 0.05-1 ng/nl and 25-50 nl were injected totaling 2.5-5 ng of RNA. For optimal expression and oocyte health, RNA was injected at the midline, the equatorial band, between animal and vegetal pole (Smart and Krishek, 1995) of stage IV oocytes.

Voltage-clamp inside-out recordings from *Xenopus* oocytes

Before recording, the outer vitelline membrane was removed by placing the oocyte in hypertonic stripping solution (in mM: 200 K$^+$ asparate, 20 KCl, 1 MgCl, 10 ethylene glycol tetra acetic acid (EGTA), 10 HEPES, pH 7.4) for a few minutes (Brown et al., 2008) and carefully peeling off the outer membrane with fine forceps avoiding cell damage. Oocytes

were then transferred into a recording chamber filled with bath solution recapitulating intracellular ion composition (in mM: 160 KCl, 0.5 MgCl$_2$, 1 EGTA, 10 HEPES, adjusted pH 7.4 with KOH). Filamented, heat polished borosillicate glass pipettes (Warner Instruments, USA; outer diameter 1.5 mm, inner diameter 1.17 mm) with 1-2 MΩ resistance were filled with pipette solution mimicking extracellular ion composition (in mM: 150 NaCl, 10 KCl, 10 HEPES, 1 MgCl$_2$, 3 CaCl$_2$, adjusted to pH 7.4 with NaOH, filtered 0.2 μm). All electrophysiology experiments were conducted at room temperature. A high seal resistance was established before the pipette was retracted rapidly ripping out a piece of membrane covering the opening of the pipette forming an inside-out patch. Electrophysiological signals were amplified by a Patch Clamp PC-501A amplifier (Warner Instruments, USA), low-pass filtered at 1 kHz, digitized at 5 kHz by a Digidata 1322A converter (Molecular Devices, USA), and acquired with Clampex 10 software (Molecular Devices, USA). A custom-made Matlab program (Mathworks, USA) was used to convert, concatenate and analyze Clampex files. A seal test (-60 to -80mV for 50 ms) verified the stability of the recording before each voltage step. A self-made line connector was used to quickly apply different solutions to the membrane patch which was guided into a polyethylene tube for fast solution exchange. Dose-response curves were created utilizing the following model equations:

$$I_c = A_1 + (A_2 - A_1)/(1 + (c/IC_{50})) \qquad \text{(Equation 1)}$$

where I_C is current at concentration c, A_1 is bottom and A_2 is top asymptote, the Matlab regression model was programmed to let $A_1 \to 0$ for $c \to$ infinity, and $A_2 \to 100$ for $c \to 0$. A non-parametric Ranksum (Mann-Wilcoxon) test was used to test the difference between the IC_{50}s.

For modelling voltage dependence of QAQ block the following equation was applied:

$$I/I_0 = (1 + [B]/K(0) \exp(-z\delta FV/RT))^{-1} \qquad \text{(Equation 2)}$$

where K(0) is the zero-voltage dissociation constant, [B] is the blocker concentration (here 100 μM), z the molecular charge (here 1), δ the fraction of the total potential drop at the binding site, F Faraday constant, R gas constant absolute temperature, and T absolute temperature (Woodhull, 1973). For the molecular charge, we used z = 1, because it is very unlikely that the two positive charges of the molecule sense the electric field of the membrane, especially in the *trans* configuration where the two ammonium groups are located about 19 Å away from each other.

Voltage-clamp whole-cell recordings from dissociated trigeminal neurons

Trigeminal ganglion (TG) neurons from neo-natal mice were prepared as described in (McKemy et al., 2002). Briefly, TGs were dissected, neurons were dissociated with collagenase and trypsin, and plated on poly(l-lysine)-coated coverslips. TG neurons were kept in minimum essential medium containing 5% horse serum, MEM vitamins (Invitrogen, USA), glutamine and penicillin-streptomycin for one night before measurements. Patch clamp recordings were performed at room temperature. Bath solution contained (in mM): 138 NaCl, 1.5 KCl, 1.2 MgCl$_2$, 2.5 CaCl$_2$, 5 HEPES and 10 glucose. Pipette solution contained (in mM): 10 NaCl, 135 K$^+$ gluconate, 10 HEPES, 2 MgCl$_2$, 2 MgATP, 1 EGTA. All solutions were adjusted to pH 7.4 and filtered 0.2 μm. Patch pipettes resistances were 2-4 MΩ. Electrophysiological measurements were performed with a Patch-Clamp PC505B amplifier (Warner Instruments, USA), digitized with a Digidata 1200 interface (Molecular Devices, USA), and low-pass–filtered at 2 kHz. Na$^+$ channel currents were corrected by P/N leak subtraction. For intracytoplasmic application through the patch pipette, QENAQ was dissolved in intracellular solution (200 μM) and measurements were started after 5−10 min of equilibration time.

Illumination for voltage-clamp experiments

Illumination of membrane patches or cells was performed by a Lambda-LS xenon lamp (Sutter Instruments, USA) with 379±17 nm and 500±8 nm band pass filters and a 125 W light source. The light beam was led through a 20x objective (Nikon Fluor, Japan, Numerical Aperture (N.A.) 0.75). Light intensities, measured at the objective using a hand-held power meter (Newport 840-C, USA), were 3.85 mW/cm^2 for 380 nm light, 4 mW/cm^2 for 480 nm light and 500 µW/cm^2 for 500 nm light.

Preparation of intact dorsal root ganglia (DRG) tissue from adult mouse

Adult mice (wild type C57BL/6J, Jackson Laboratory, on regular diet, housed in a mouse facility approved by OLAC of UC Berkeley) were deeply anesthetized with isoflurane and quickly sacrificed by cervical dislocation. The skin covering the dorsal side of the mouse was removed and the peripheral sciatic nerves were isolated from the surrounding muscle. Fibers were transected about 5 mm distal to the sciatic plexus preserving about 2.5-3 cm of total nerve fiber. Following transection the spinal column from the upper cervical vertebrae to the lower lumbar region was carefully detached from the mouse and placed in cold (4°C) artificial cerebrospinal fluid solution (ACSF, buffered at pH 7.4, in mM: 124 NaCl, 4 KCl, 2 MgCl$_2$, 2 CaCl$_2$, 26 NaHCO$_3$, 20 D-glucose, 2 Na Pyruvate, 0.4 Ascorbic Acid), constantly equilibrated with 95% O$_2$ and 5% CO$_2$. A laminectomy from the thorax to the sacrum revealed the spinal column which was subsequently removed exposing the DRGs. Finally, bone structures of the spinal column were gently opened to take out the lumbar L3 - L6 DRGs. Only the most outer layer of the epineurium was removed, leaving the tissue intact otherwise. After dissection, the DRG preparations were placed on a floating nitrocellulose membrane (Sartorius Stedim Biotech, USA) in an oxygenation chamber keeping the tissue at the air-solution interface of equilibrated ACSF at room temperature (18-22°C) to recover for 30-60 min before the start of recordings.

Multi electrode array recordings from intact dorsal root ganglia

Intact DRG tissue was mounted onto a multi electrode array (MEA) chip (MEA60-200 3D GND, Qwane Bioscience, Switzerland) consisting of sixty 3D tip-shaped platinum electrodes penetrating 60 µm into tissue spaced at 200 µm (Heuschkel et al., 2002). The tissue is secured in place to ensure optimal contact using a 'harp' made from dialysis membrane stretched over thick platinum wire and bonded with super glue; the wire was U-shaped to allow the nerve to exit without being crushed. The MEA chip was mounted on an MEA1060-UP-BC amplifier (Multi Channel Systems, Germany) and placed on the stage of an upright microscope (Labophot-2, Nikon, Japan). Peripheral nerves were electrically stimulated using a suction electrode driven by an external, battery driven DS2 stimulus isolator (Digitimer, UK). The nerve bundle was gently led into a manipulator-mounted glass suction electrode of appropriate size. Stimulation mode (constant current vs. constant voltage), blanking time of the amplifier (200-2000 µs), stimulus pulse length (20-600 µs) and stimulation strength were optimized to yield extracellular responses with maximal response amplitude while minimizing electrical artifacts at the beginning of recordings. DRGs were checked for response to stimulation at 1 Hz prior to recording. Evoked responses were recorded at 20 kHz sampling rate with MC_Rack v4.5.12 software (Multi Channel Systems, Germany). Raw voltage traces were filtered with a second order Butterworth high pass filter at 300 Hz and a low pass filter of 10 kHz. Illumination was provided by a Spectra-LCR-3X-A2 LED light source (Lumencor, USA) routed through a 4x objective (N.A. 0.13, Nikon, Japan), yielding an intensity of 13.2 mW/cm^2 for 475 nm light. Stimulator, recording software and light source were centrally controlled by a custom made Matlab (MathWorks, USA) program triggering TTL pulses through a BNC-2110 I/O card (National Instruments,

USA). The MEA chamber was continuously perfused with oxygenated ACSF at about 3 ml/min and recordings were performed at constant 34°C. QENAQ was incubated at 300 μM solution in ACSF for 5 min. DRGs were washed with ACSF for 10 min after incubation before experiments. Recordings were done at a stimulation rate of 10 Hz while illuminating the DRG with 480 nm light or in darkness. The start of recordings was synchronized to the onset of the stimulus pulse and recordings lasted 50 to 90 ms for each stimulation sweep. Each experiment consisted of five cycles of 30 s under 480 nm light followed by 30 s in the dark. The DRG was stimulated for the last 5 s under illumination or in the dark, allowing 25 s to recover from adaptation in between stimulation episodes.

Analysis of multi-electrode data

Multi electrode data was imported into Matlab using the import functionality of the FIND program bundle (University of Freiburg, Germany; (Meier et al., 2008)). Subsequent analysis was performed by a custom made Matlab program package. Stimulation artifacts were excluded from the analysis and evoked signals were detected by a threshold manually set beyond the noise level. Overall responses were divided in negative and positive deflections and each deflection was analyzed separately. A Matlab algorithm conservatively excluded small and/or irregular signals. We chose the area under the voltage trace as parameter to calculate photosensitivity. This value was averaged over the five recording cycles in each wavelength. Since QAQ and QENAQ function as an open channel blocker (Mourot et al., 2012), photosensitivity increases over the duration of a stimulation episode. Therefore, the last 1.5 s of the stimulation protocol were used to calculate a measure of normalized photosensitization, the Photoswitching Index (PI), which is defined as (area in 480nm – area in dark) / (area in 480nm + area in dark). The distribution of PI values followed a non-normal distribution and we therefore applied the non-parametric Mann-Whitney u-test (for two comparisons) or the Kruskal Wallis test with Dunn's post hoc test (for more than two comparisons).

Molecular docking i*n silico*

The three-dimensional structure of the open channel Kv1.2-2.1 chimera (PDB ID 2R9R, (Long et al., 2007) were used to dock *cis* and *trans* QAQ molecules into the lumen of the channel. Molecular docking was carried out in Glide 5.7 (Halgren et al., 2004) implemented in Maestro 9.2 (Schrodinger Inc., USA). The x-ray structure was used to create a grid after the addition of hydrogen atoms and the removal of non-protein moieties. A QAQ 3D structure (*cis* or *trans* configuration) was docked into this grid using the Standard Precision algorithm.

Nomenclature of targets and ligands

Key protein targets and ligands in this article are hyperlinked to corresponding entries in http://www.guidetopharmacology.org, the common portal for data from the IUPHAR/BPS Guide to PHARMACOLOGY (Southan et al., 2016), and are permanently archived in the Concise Guide to PHARMACOLOGY 2015/16 (Alexander et al., 2015a; 2015b).

- Results

Concentration dependence of QAQ blockade

Intracellular QAQ blocks voltage-gated K^+, Na^+ and Ca^{2+} channels in darkness (Mourot et al., 2012). To investigate QAQ binding to the internal TEA binding site, we have used the Shaker-inactivation removed (Shaker-IR) K^+ channel, a mutant that does not inactivate during brief depolarization (Hoshi et al., 1990; Demo and Yellen, 1991). This channel lacks the N-terminal "ball and chain" motif, which by binding to the internal TEA binding site (Zhou et al., 2001) might interfere with QAQ blockade. Because QAQ does not cross the lipid bilayer (Mourot et al., 2012), we used the inside-out configuration from excised patches to directly expose the photoswitchable blocker to the cytosolic side of Shaker-IR, and characterize *cis* and *trans* QAQ blockade (Fig. 2A). Shaker-IR opening was triggered with depolarizing voltage steps (-60 to +40 mV) for 200 ms at 1 Hz. QAQ was applied until blockade of current reached steady-state (Fig. 2B). Then, QAQ was photoisomerized to *cis* using 380 nm light, which resulted in a rapid increase in K^+ current. Illumination with 500 nm light reverted QAQ to *trans* and restored blockade. Using 100 μM QAQ, 61.0±5.5 % of the Shaker-IR steady-state current (Iss) was blocked under green light, and blockade was reduced to 16.4±3.8 % under 380 nm light (Fig. 2C, D). At this illumination condition, >96% of the QAQ molecules are converted to *cis* (Mourot et al., 2013b). Hence, while both isomers of QAQ can block Shaker-IR current, the effect is more profound in *trans* than in *cis*. A full dose-response curve of steady-state current blockade showed that *trans* QAQ has a six-fold lower IC_{50} value (65 ± 17 μM) compared to *cis* QAQ (380 nm light: >96% *cis*, IC_{50} = 390 ± 111 μM, p = 0.008 Mann-Wilcoxon test, Fig. 2D).

Voltage dependence of QAQ blockade

Because QAQ is a charged molecule, its interaction with K^+ channels may be sensitive to the electric field across the membrane. We investigated the effect of membrane potential on *cis* and *trans* QAQ block with incremental voltage steps from -80 to +40 mV (Fig. 3A). QAQ blockade was more potent under 500 nm than 380 nm light, for all membrane potentials tested (Fig. 3A, B). To quantify the voltage-dependence of blockade, we measured the reduction in current by both *trans* and *cis* QAQ (100 μM) at voltages where channel activation is complete, i.e. >-20 mV (see black trace in Fig. 3C). Blockade with *trans* QAQ was slightly voltage-dependent and favoured by more positive potentials (Fig. 3C). Voltage dependence of block can be described by the 'effective valence' value, and the fraction δ of the membrane potential QAQ traverses to reach its binding site (Woodhull, 1973). A fit of equation 2 (see methods) yields δ_{trans}= 0.18, which agrees closely with the δ value (0.15) reported for TEA block on K^+ channels (French and Shoukimas, 1981; Yellen et al., 1991). In contrast, blockade with *cis* QAQ was not voltage dependent and was fitted with a linear regression (m_{cis} = 0.0004 mV^{-1}, n.s. to m = 0 with p = 0.32, Student's t test). This suggests that *cis* QAQ blocks K^+ current, but without sensing the electrical field of the membrane.

Use- and time-dependence of QAQ blockade

A common property of quaternary ammonium pore blockers is that they bind to the pore only after the channel has opened (Choi et al., 1993). To test whether this is true for *cis* and

trans QAQ, we have perfused 300 μM QAQ under 380 or 500 nm light for one minute, while keeping the membrane potential at -60 mV to ensure a very low opening probability. This perfusion time is normally sufficient to achieve potent blockade (Fig. 2B). Shaker-IR currents were then monitored at 1Hz (+40 mV depolarization pulses), under both wavelengths of light, and compared with currents recorded before QAQ application. The first depolarizing test pulse elicited a nearly-full sized I_{ss} current, but block rapidly accumulated over time with subsequent pulses under both wavelengths of light similar to QAQ application while Shaker is constantly opened (Fig. 4A). This indicates that neither *cis* nor *trans* QAQ has access to the pore of Shaker-IR while the channel is closed. Like other quaternary ammonium pore blockers, QAQ produced a use-dependent accumulative blockade in response to a train of depolarizing pulses, under both wavelengths of light (Fig. 4B). Higher frequencies produced more blockade for both *cis* and *trans* QAQ, while blockade with *cis* QAQ was negligible for frequencies <1 Hz. Hence, increased opening of K^+ channels allows increased access of QAQ to the pore. The blockade of both *cis* and *trans* QAQ was also time dependent, i.e., blockade developed non-instantaneously during a voltage pulse (Fig. 4C), which corresponds to the association of QAQ to the open channel. The current block with *trans* QAQ followed an exponential decline and increased with QAQ concentration (Fig. 4D), similar to other open-channel blockers, including long alkyl-chain quaternary ammonium (Choi et al., 1993) and the N-terminal ball and chain motif of K^+ channels (Demo and Yellen, 1991). In contrast, the blockade of *cis* QAQ could not be fitted with an exponential function.

Interaction of QAQ with the gating mechanism of Shaker-IR

We next tested whether QAQ interacts with the gating mechanism of the Shaker-IR channel. Most quaternary ammonium blockers don't affect the activation kinetics of the channel, but slow down deactivation because they must dissociate before the channel can close (Armstrong, 1971; Choi et al., 1993; Holmgren et al., 1997). Similarly, we found that the activation kinetics of Shaker-IR were not affected by the presence of QAQ, in either wavelength (see Fig. 2C for instance). To look at deactivation kinetics, we measured the exponential decline in tail current after repolarization to -60 mV and found that channel closing was indeed slowed when *cis* QAQ was bound to the pore (Fig. 4E), consistent with a "foot in the door" mechanism (Armstrong, 1971). Surprisingly, *trans* QAQ had no significant effect on channel deactivation kinetics, which may indicate a faster dissociation kinetics of the elongated trans isomer, compared to the bent *cis* QAQ.

Binding modes of *cis* and *trans* QAQ

The two QAQ isomers block Shaker-IR K^+ channel with different potency, voltage-dependence and time-dependence, and only the *cis* isomer affects channel gating, suggesting that *cis* and *trans* QAQ bind the internal lumen with distinct orientations. The crystal structure of the K^+ channel might provide additional insights into light-dependent QAQ blockade. We used a docking simulation to explore the predicted fit of *cis* or *trans* QAQ to a chimeric K^+ channel, whose pore domain is derived from Kv1.2, a mammalian homologue of Shaker (Long et al., 2007). This channel was crystallized in the open conformation, which should allow QAQ access and binding. Figure 5 shows one of the best docking poses for each isomer. In the *trans* configuration, a quaternary ammonium of QAQ is directly beneath the selectivity filter, on the central 4-fold axis of the channel (Fig. 5A, B). The second quaternary ammonium is directed away toward the exit, while the azobenzene interacts with

hydrophobic residues from the S5 and S6 helices. This pose is similar to quaternary ammonium blockers complexed with the KcsA K$^+$ channel (Zhou et al., 2001; Lenaeus et al., 2005; Faraldo-Gómez et al., 2007) and is consistent with electrophysiology experiments indicating two functionally distinct subsites for blockers with a TEA headgroup and an hydrophobic tail (Baukrowitz and Yellen, 1996). Binding of *cis* QAQ was drastically different: due to its bent configuration, this isomer failed to position a charged ammonium in a central position below the selectivity filter, in none of the best poses (Fig. 5 A, B). These *in silico* results are in agreement with our electrophysiology providing a plausible explanation for why blockade of *cis* QAQ is less potent (Fig. 2D) and not voltage sensitive (Fig. 3C).

Tuning the photo-physical properties of QAQ

QAQ has been used *in vivo* as an optically-regulated local anaesthetic, yet only in the cornea which is fully transparent, thereby facilitating light access. Optical control of nociception in the skin or deeper into organ tissues requires a QAQ derivative that photoswitches at longer wavelengths of light. The photosensitive core of QAQ (Fig. 1A) is made of a "classical" azobenzene group flanked with two mildly electron-withdrawing acylamino moieties. In the dark, *trans* QAQ predominates, with a strong π-π* band at 362 nm in water (Fig. 6B). Irradiation with near UV light (380 nm) isomerizes the azobenzene group to the higher-energy *cis* conformer. *Cis* QAQ is metastable, and relaxes to the lower-energy *trans* state in the dark, with a half-life of 7-8 min (Mourot et al., 2012). Isomerization back to *trans* can be accelerated upon irradiation with a longer wavelength of light (500 nm). The limitation of using UV light for *in vivo* and therapeutic applications prompted us to design a red-shifted version of QAQ. The incorporation of electron-donating groups in the *ortho* position of the azobenzene ring shifts the wavelength for maximal photoswitching to a longer wavelength and increases the rate of spontaneous cis to *trans* relaxation in the dark (Beharry et al., 2011; Fehrentz et al., 2012; Samanta et al., 2013), for review see (Dong et al., 2015). Yet efficient red shifting is achieved with the introduction of bulky electron-donating substituents, which can impair the binding of the ligand moiety to the protein (Fehrentz et al., 2012). Azobenzenes with an electron-donating group in the *para* position also absorb at longer wavelengths of light (blue range) and display fast kinetics of thermal relaxation in the dark (ms-s) (Sadovski et al., 2009; Mourot et al., 2011; Kienzler et al., 2013). We reasoned that the steric hindrance induced by a *para* substitution might be better tolerated than that induced by an *ortho* substitution, and that ion channel blockade might be less affected. We designed a red-shifted version of QAQ (QENAQ) with minimal variation to the structure, by replacing the electron-withdrawing acylamino with an electron-donating ethylamino group in the *para* position (Fig. 6A). QENAQ was synthetized as depicted in Scheme 1. As expected, QENAQ displayed a red shift in its absorption spectrum by about 80 nm (λ_{max} = 445 nm) in aqueous solution (Fig. 6B), similar to what has been observed for related red-shifted K$^+$ channel blockers (Mourot et al., 2011).

QENAQ photosensitizes native voltage-gated K$^+$ and Na$^+$ channels.

QAQ blocks not only K$^+$ channels but also Na$^+$ and Ca^{2+} channels (Mourot et al., 2012). The initial red-shifted compounds we had designed were potent K$^+$ channel blockers but failed at photosensitizing Na$^+$ channels and therefore could not silence neurons (Mourot et al., 2011). To test whether QENAQ photosensitizes voltage-gated Na$^+$ and K$^+$ channels, we included it in the patch pipette, to allow direct access of the drug to the cytoplasmic binding site. Voltage-gated Na$^+$ current from primary sensory neurons were recorded under 480 nm light and in darkness. We found that Na$^+$ currents were larger under blue light, when QENAQ

(200 µM) was partially in *cis*, than in darkness, when QENAQ was fully in *trans* (Fig. 7A). Illumination with blue light rapidly increased current, while blocking was restored within seconds in darkness (Fig. 7B). We initially tested the concentration used for QAQ (100 µM) but did not observe reliable photoswitching (not shown). QENAQ (200 µM) also photosensitized native voltage-gated K^+ channels from primary sensory neurons. K^+ currents were larger under blue light than in darkness (Fig. 7C) and blockade occurred within seconds after light was shut off (Fig. 7D). Hence, like QAQ, QENAQ blocks voltage-gated K^+ and Na^+ channels in the *trans* configuration and unblocks them in *cis*. But unlike QAQ, conversion to *cis* occurred upon illumination with visible light, instead of near-UV light needed for QAQ. In addition, *cis* QENAQ is not thermally stable in the dark, and conversion back to *trans* occurs spontaneously, within seconds as judged by the recurrence of Na^+ and K^+ channel blockade. Hence a single wavelength of light, in the blue range, is required to rapidly toggle QENAQ in and out of its binding site on ion channels.

QENAQ photosensitizes intact dorsal root ganglion neurons

QENAQ, like QAQ, photosensitizes voltage-gated Na^+ and K^+ channels in primary sensory neurons. To check whether QENAQ could be used to optically control the electrical activity of these neurons, we turned to a system we have developed for QAQ (Mourot et al., 2012). We recorded the activity of tens of sensory neurons at once within an intact DRG, while simultaneously controlling the isomeric state of the photoswitch using the optics of a microscope (Fig. 8A). Whole intact DRGs were placed on a 3-dimensional MEA, consisting of 60 spine-shaped electrodes that protrude into the ganglion (Fig. 8B). Neuronal activity was evoked by electrically stimulating action potentials in axons of the peripheral nerve. Each electrode recorded the integrated extracellular activity of several neurons, appearing as a Compound Action Potential (CAP, Fig. 8C). Most signals recorded originate from C-fiber neurons, including nociceptors, which can be identified by their slow-conduction velocity (Mourot et al., 2012). After treatment with QENAQ, the amplitude of evoked CAPs was larger in 480 nm light than in darkness (Fig. 8C, D). Moreover, the CAP amplitude diminished more rapidly in darkness than in 480 nm light during a stimulus train (Fig. 8D, E), consistent with cumulative activity-dependent blockade of voltage-gated channels. Photosensitivity was quantified by a measure called Photoswitch Index (PI) of firing (Fig. 8E inset and methods), which reflects the amount of photoswitch compound loaded into neurons. QAQ is a membrane-impermeant molecule, yet it can enter neurons by passing through open TRPV1 channels or other conduit channels that open transiently in dissected DRGs (Mourot et al., 2012). Similarly, QENAQ alone photosensitized neurons, while application of the TRPV1 agonist capsaicin (1 µM) promoted QENAQ loading into neurons, as shown by an increased PI (Fig. 8F). Hence, QENAQ could accumulate in neurons through activated nociceptive ion channels and enabled photo-control of action potential firing with visible light.

- Discussion

QAQ and QENAQ are potent photoswitchable blockers of voltage-gated K^+ and Na^+ channels. They provide non-invasive and rapid silencing of firing by pain-sensing neurons and therefore offer promise both for understanding and for treating pain. As a consequence, characterizing the biophysics of QAQ binding to voltage-gated ion channels may increase the utility of QAQ as a fundamental research tool, while rationally tuning the photochemical properties of QAQ should improve the translational value of such compounds.

Mechanism of QAQ blockade

We found that both isomers of QAQ are use-dependent open-channel blockers for voltage-gated K^+ channels. The mechanism of *trans* QAQ block resembles that of hydrophobic quaternary ammonium blockers, with a slight voltage-dependence, possibly due to the positioning of the TEA group just beneath the selectivity filter. The mechanism of *cis* QAQ blockade is quite different: it shows no voltage-dependence, in agreement with the TEA groups positioned away from the central path for K^+ ions. *Cis* QAQ is less potent than *trans* QAQ at blocking ion conduction. This can be explained either by a decreased affinity, or by a decreased efficacy of block of the *cis* isomer, or both. The fact that *cis* QAQ drastically affects the closing kinetics of the channel at a concentration (100 μM) that yields only 16% block favours the hypothesis of *cis* QAQ occupying the lumen, yet blocking K^+ conduction inefficiently. This hypothesis is also in agreement with our docking simulations and an unusual binding of the quaternary ammonium groups. However, since we technically were unable to perfuse *cis* QAQ at a saturating concentration (Fig. 2D), we could not verify whether blockade with *cis* QAQ is complete or not, and therefore we cannot completely rule out the possibility that the affinity of *cis* QAQ is lower than that of *trans* QAQ. QAQ is 6-fold more potent in blocking K^+ channels in the *trans* than in the *cis* configuration. This is significantly less than light-dependent block by two other azobenzene photoswitches AAQ or BzAQ (30- and 60-fold *trans*/cis blocking ratio, respectively) (Banghart et al., 2009). A large difference in IC50 between the two isomers is important to avoid residual blockade with the *cis* isomer, for a large range of concentrations. Nevertheless, the appropriate concentration (100 μM) stimulation frequency (<1Hz) and sufficiently bright light can ensure no blockade of K^+ channels in 380 nm light and nearly complete block in 500 nm light (see Fig. 4B). Similarly, 100 μM QAQ ensures no block of Na^+ channels in the dark and nearly full unblock in 380 nm light at low frequency stimulation (Mourot et al., 2012). Together, these actions on channels enable reversible control of action potential firing.

Silencing primary sensory neurons with light

Optical silencing of nociceptor firing can also been achieved through exogenous expression of optogenetic tools (Montgomery et al., 2016). Genetic strategies can be used to restrict opsin expression to a subset of neurons, e.g. to nociceptors expressing voltage-gated Nav1.8 Na^+ channels (Daou et al., 2013) or TRPV1 receptors (Li et al., 2015). Intrasciatic viral injection of AAV6 viruses carrying inhibitory opsins has been shown to selectively transduce nociceptors in wild type animals, resulting in effective optical inhibition of acute pain, even though only a small fraction of nociceptors could be transduced (Iyer et al., 2014). Our method for silencing neurons is different: QAQ and QENAQ block the intrinsic neuronal ion channels that are responsible for the initiation and propagation of action potentials. We found that the mechanism of QAQ blockade is indeed very similar to that of classical local anaesthetics (Hille, 2001; Fozzard et al., 2011), which are highly potent pain killers. QAQ and QENAQ block both K^+ and Na^+ channels, reducing action potential amplitude and increasing its half-width (Mourot et al., 2012). Broadening action potentials increases the open time of Na^+ channels, potentiating channel blockade and resulting in a net inhibition of neuronal activity (Drachman and Strichartz, 1991). QAQ, which potently photosensitizes ion channels at a concentration of 100 μM, is slightly more potent than QENAQ. Yet both molecules can be applied to study neuronal systems similar to QX-314 while adding the ability to precisely photo-control ion channel blockade. QAQ and QENAQ photosensitize native tissue within minutes, as opposed to days or weeks for viral expression of opsins. And because they are highly soluble small molecules, QAQ and QENAQ diffuse readily through tissue, reaching all cells that are susceptible to photosensitization.

Red shifting QAQ for safer, potent optical control deep into tissue

Light penetration through biological tissue critically depends on the wavelength, with short wavelengths being scattered and absorbed more strongly (Yizhar et al., 2011). QENAQ has a red-shifted absorbance spectrum and therefore photoswitches with visible light, which should facilitate control with transdermal illumination. In addition, because QENAQ relaxes back to *trans* rapidly in the dark (seconds), only a single wavelength is required for rapidly switching the molecule between its active and inactive forms. As a downside, continuous high intensity light is required to reduce the concentration of the *trans* isomer sufficient to relieve blockade. However, a derivative of QENAQ with a higher thermal stability, as has been achieved with a *ortho*-substituted QAQ derivatives (half-life of the *cis* isomer from hours to days) (Mourot et al., 2013b) would be an ideal candidate for long-lasting optical control of pain signalling. A major issue remains light delivery in the periphery, where classical optical fibers are not suitable. Multiple technologies are emerging, including wirelessly powered miniature LEDs (Kim et al., 2013; Montgomery et al., 2015; Park et al., 2015) and wireless optofluidic systems for localized drug delivery and photostimulation (Jeong et al., 2015). This latter system could prove extremely useful for optopharmacology applications using QENAQ or other photosensitive drugs.

Potential clinical implications for chronic pain

The emergence of optopharmacology offers interesting therapeutic promise in pain research, by achieving high temporal and spatial precision of drug action (Lerch et al., 2016). Several photo-pharmacological agents have been introduced targeting specific transduction channels and neurotransmitter receptors in the pain pathway, including TRPV1 agonists and antagonists (Stein et al., 2013; Frank et al., 2015), a μ-opioid receptor agonist (Schönberger and Trauner, 2014), a propofol-derived anaesthetic (Stein et al., 2012) and an allosteric modulator of metabotropic glutamate receptor 4 (Zussy et al., 2016). QAQ and QENAQ represent a different strategy for achieving optical control over nociception. While these compounds act on voltage-gated ion channels found in all neurons, they only enter and accumulate in nociceptors, which have large-pore ion channels such as TRPV1. This gives QAQ and QENAQ potentially interesting clinical value for controlling chronic pain while simultaneously minimizing unwanted side effects in other neurons. Indeed, it has been shown that, in animal models of neuropathic pain, TRPV1 channels are hyperactive in central terminals of the dorsal horn (Kim et al., 2014). Hence, by exploiting this cell-entry mechanism, QAQ and QENAQ could be self-targeted to hyper-active neurons, i.e. the ones that need to be silenced the most, and afford pain-selective analgesia. In addition, because ion channel blockade can be finely tuned with light intensity and/or wavelength, analgesia could potentially be photo-titrated at will. QAQ and QENAQ may not fulfill all the prerequisites for clinical use. In particular, it will be important to develop compounds with greater IC_{50} difference between the two isomers and that can be photo-isomerized in both directions with wavelengths of light in therapeutic window (600-1200 nm). Nevertheless, QAQ and QENAQ represent a useful starting point for the development of light-switchable local anaesthetics.

- Author contributions

- Acknowledgments

- Conflict of interest statement

RHK is a SAB member and consultant of Photoswitch Biosciences, Inc., which is developing commercial uses for chemical photoswitches.

- References

Alexander, S., Catterall, W.A., and Kelly, E. (2015a). The Concise Guide to PHARMACOLOGY 2015/16: Voltage-gated ion channels. British Journal of ….

Alexander, S.P., Peters, J.A., Kelly, E., Marrion, N., Benson, H.E., Faccenda, E., et al. (2015b). The Concise Guide to PHARMACOLOGY 2015/16: Ligand-gated ion channels. British Journal of Pharmacology *172*: 5870–5903.

Armstrong, C.M. (1971). Interaction of tetraethylammonium ion derivatives with the potassium channels of giant axons. J Gen Physiol *58*: 413–437.

Banghart, M.R., Mourot, A., Fortin, D.L., Yao, J.Z., Kramer, R.H., and Trauner, D. (2009). Photochromic Blockers of Voltage-Gated Potassium Channels. Angew. Chem. Int. Ed. Engl. *48*: 9097–9101.

Baukrowitz, T.T., and Yellen, G. (1996). Two functionally distinct subsites for the binding of internal blockers to the pore of voltage-activated K+ channels. Proceedings of the National Academy of Sciences *93*: 13357–13361.

Beharry, A.A., Sadovski, O., and Woolley, G.A. (2011). Azobenzene Photoswitching without Ultraviolet Light. J. Am. Chem. Soc. *133*: 19684–19687.

Binshtok, A.M., Bean, B.P., and Woolf, C.J. (2007). Inhibition of nociceptors by TRPV1-mediated entry of impermeant sodium channel blockers. Nature *449*: 607–610.

Binshtok, A.M., Gerner, P., Oh, S.B., Puopolo, M., Suzuki, S., Roberson, D.P., et al. (2009).

Coapplication of lidocaine and the permanently charged sodium channel blocker QX-314 produces a long-lasting nociceptive blockade in rodents. Anesthesiology *111*: 127–137.

Brown, A.L., Johnson, B.E., and Goodman, M.B. (2008). Patch Clamp Recording of Ion Channels Expressed in Xenopus Oocytes. JoVE.

Choi, K.L., Mossman, C.C., Aubé, J.J., and Yellen, G. (1993). The internal quaternary ammonium receptor site of Shaker potassium channels. Neuron *10*: 533–541.

Daou, I., Tuttle, A.H., Longo, G., Wieskopf, J.S., Bonin, R.P., Ase, A.R., et al. (2013). Remote Optogenetic Activation and Sensitization of Pain Pathways in Freely Moving Mice. J. Neurosci. *33*: 18631–18640.

Demo, S.D.S., and Yellen, G. (1991). The inactivation gate of the Shaker K+ channel behaves like an open-channel blocker. Neuron *7*: 743–753.

Dong, M., Babalhavaeji, A., Samanta, S., Beharry, A.A., and Woolley, G.A. (2015). Red-Shifting Azobenzene Photoswitches for in Vivo Use. Acc. Chem. Res. *48*: 2662–2670.

Drachman, D.D., and Strichartz, G.G. (1991). Potassium channel blockers potentiate impulse inhibition by local anesthetics. Anesthesiology *75*: 1051–1061.

Faraldo-Gómez, J.D., Kutluay, E., Jogini, V., Zhao, Y., Heginbotham, L., and Roux, B. (2007). Mechanism of Intracellular Block of the KcsA K+ Channel by Tetrabutylammonium: Insights from X-ray Crystallography, Electrophysiology and Replica-exchange Molecular Dynamics Simulations. Journal of Molecular Biology *365*: 649–662.

Fehrentz, T., Kuttruff, C.A., Huber, F.M.E., Kienzler, M.A., Mayer, P., and Trauner, D. (2012). Exploring the Pharmacology and Action Spectra of Photochromic Open-Channel Blockers. ChemBioChem *13*: 1746–1749.

Fehrentz, T., Schönberger, M., and Trauner, D. (2011). Optochemical Genetics. Angew. Chem. Int. Ed. Engl. *50*: 12156–12182.

Fozzard, H.A., Sheets, M.F., and Hanck, D.A. (2011). The sodium channel as a target for local anesthetic drugs. Front Pharmacol *2*: 68.

Frank, J.A., Moroni, M., Moshourab, R., Sumser, M., Lewin, G.R., and Trauner, D. (2015). Photoswitchable fatty acids enable optical control of TRPV1. Nature Communications *6*: 1–11.

French, R.J., and Shoukimas, J.J. (1981). BLOCKAGE OF SQUID AXON POTASSIUM CONDUCTANCE. Biophysical Journal *34*: 271–291.

Halgren, T.A., Murphy, R.B., Friesner, R.A., Beard, H.S., Frye, L.L., Pollard, W.T., et al. (2004). Glide: A New Approach for Rapid, Accurate Docking and Scoring. 2. Enrichment Factors in Database Screening. J. Med. Chem. *47*: 1750–1759.

Heuschkel, M.O., Fejtl, M., Raggenbass, M., Bertrand, D., and Renaud, P. (2002). A three-dimensional multi-electrode array for multi-site stimulation and recording in acute brain slices. Journal of Neuroscience Methods *114*: 135–148.

Hille, B.B. (2001). Ion Channels of Excitable Membranes (3rd Edition) (Sinauer Associates Inc 2001).

Holmgren, M.M., Smith, P.L., and Yellen, G. (1997). Trapping of organic blockers by closing of voltage-dependent K+ channels: evidence for a trap door mechanism of activation gating. J Gen Physiol *109*: 527–535.

Hoshi, T., Zagotta, W.N., and Aldrich, R.W. (1990). Biophysical and molecular mechanisms of Shaker potassium channel inactivation. Science *250*: 533–538.

Iyer, S.M., Montgomery, K.L., Towne, C., Lee, S.Y., Ramakrishnan, C., Deisseroth, K., et al. (2014). Virally mediated optogenetic excitation and inhibition of pain in freely moving nontransgenic mice. Nature Biotechnology 1–8.

Jeong, J.-W., McCall, J.G., Shin, G., Zhang, Y., Al-Hasani, R., Kim, M., et al. (2015). Wireless Optofluidic Systems for Programmable In Vivo Pharmacology and Optogenetics. Cell 1–14.

Kienzler, M.A., Reiner, A., Trautman, E., Yoo, S., Trauner, D., and Isacoff, E.Y. (2013). A red-shifted, fast-relaxing azobenzene photoswitch for visible light control of an ionotropic glutamate receptor. J. Am. Chem. Soc. *135*: 17683–17686.

Kim, T.I., McCall, J.G., Jung, Y.H., Huang, X., Siuda, E.R., Li, Y., et al. (2013). Injectable, Cellular-Scale Optoelectronics with Applications for Wireless Optogenetics. Science *340*: 211–216.

Kim, Y.S., Chu, Y., Han, L., Li, M., Li, Z., LaVinka, P.C., et al. (2014). Central Terminal Sensitizationof TRPV1 by Descending Serotonergic Facilitation Modulates Chronic Pain. Neuron *81*: 873–887.

Kramer, R.H., Mourot, A., and Adesnik, H. (2013). Optogenetic pharmacology for control of native neuronal signaling proteins. Nature Neuroscience *16*: 816–823.

Lenaeus, M.J., Vamvouka, M., Focia, P.J., and Gross, A. (2005). Structural basis of TEA blockade in a model potassium channel. Nature Structural & Molecular Biology *12*: 454–459.

Lerch, M.M., Hansen, M.J., van Dam, G.M., Szymański, W., and Feringa, B.L. (2016). Emerging Targets in Photopharmacology. Angew. Chem. Int. Ed. Engl. *55*: 10978–10999.

Li, B., Yang, X.-Y., Qian, F.-P., Tang, M., Ma, C., and Chiang, L.-Y. (2015). A novel analgesic approach to optogenetically and speci. Brain Research *1609*: 12–20.

Long, S.B., Tao, X., Campbell, E.B., and MacKinnon, R. (2007). Atomic structure of a voltage-dependent K+ channel in a lipid membrane-like environment. Nature *450*: 376–382.

McGrath, J.C., and Lilley, E. (2015). Implementing guidelines on reporting research using animals (ARRIVE etc.): new requirements for publication in BJP. British Journal of Pharmacology.

McKemy, D.D.D., Neuhausser, W.M.W., and Julius, D. (2002). Identification of a cold receptor reveals a general role for TRP channels in thermosensation. Nature *416*: 52–58.

Meier, R., Egert, U., Aertsen, A., and Nawrot, M.P. (2008). FIND — A unified framework for neural data analysis. Neural Networks *21*: 1085–1093.

Montgomery, K.L., Iyer, S.M., Christensen, A.J., Deisseroth, K., and Delp, S.L. (2016). Beyond the brain: Optogenetic control in the spinal cord and peripheral nervous system. Sci Transl Med *8*: 337rv5.

Montgomery, K.L., Yeh, A.J., Ho, J.S., Tsao, V., Iyer, S.M., Grosenick, L., et al. (2015). Wirelessly powered, fully internal optogenetics for brain, spinal and peripheral circuits in mice. Nature Methods 1–10.

Mourot, A., Fehrentz, T., and Kramer, R.H. (2013a). Photochromic Potassium Channel Blockers: Design and Electrophysiological Characterization. In Methods in Molecular Biology, (Totowa, NJ: Humana Press), pp 89–105.

Mourot, A., Fehrentz, T., Le Feuvre, Y., Smith, C.M., Herold, C., Dalkara, D., et al. (2012). Rapid optical control of nociception with an ion-channel photoswitch. Nature Methods *9*: 396–402.

Mourot, A., Kienzler, M.A., Banghart, M.R., Fehrentz, T., Huber, F.M.E., Stein, M., et al. (2011). Tuning Photochromic Ion Channel Blockers. ACS Chem. Neurosci. *2*: 536–543.

Mourot, A., Tochitsky, I., and Kramer, R.H. (2013b). Light at the end of the channel: optical manipulation of intrinsic neuronal excitability with chemical photoswitches. Front. Mol. Neurosci. *6*: 1–15.

Park, Il, S., Brenner, D.S., Shin, G., Morgan, C.D., Copits, B.A., Chung, H.U., et al. (2015). soft, stretchable, fully implantable miniaturized optoelectronic systems for wireless optogenetics. Nature Biotechnology *33*: 1280–1286.

Polosukhina, A., Litt, J., Tochitsky, I., Nemargut, J., Sychev, Y., De Kouchkovsky, I., et al. (2012). Photochemical Restoration of Visual Responses in Blind Mice. Neuron *75*: 271–282.

Sadovski, O., Beharry, A.A., Zhang, F., and Woolley, G.A. (2009). Spectral Tuning of Azobenzene Photoswitches for Biological Applications. Angew. Chem. Int. Ed. Engl. *48*: 1484–1486.

Samanta, S., Beharry, A.A., Sadovski, O., McCormick, T.M., Babalhavaeji, A., Tropepe, V., et al. (2013). Photoswitching azo compounds in vivo with red light. J. Am. Chem. Soc. 130610143333001.

Schönberger, M., and Trauner, D. (2014). A Photochromic Agonist for μ-Opioid Receptors. Angew. Chem. Int. Ed. Engl. *53*: 3264–3267.

Smart, T.G., and Krishek, B.J. (1995). Xenopus Oocyte Microinjection and Ion-Channel Expression. In Neuromethods: Patch-Clamp Applications and Protocols, A. Boulton, G. Baker, and W. Walz, eds. pp 259–305.

Southan, C., Sharman, J.L., Benson, H.E., Faccenda, E., Pawson, A.J., Alexander, S.P.H., et al. (2016). The IUPHAR/BPS Guide to PHARMACOLOGY in 2016: towards curated quantitative interactions between 1300 protein targets and 6000 ligands. Nucleic Acids Research *44*: D1054–D1068.

Stein, M., Breit, A., Fehrentz, T., Gudermann, T., and Trauner, D. (2013). Optical Control of TRPV1 Channels. Angew. Chem. Int. Ed. Engl. n/a–n/a.

Stein, M., Middendorp, S.J., Carta, V., Pejo, E., Raines, D.E., Forman, S.A., et al. (2012). Azo-Propofols: Photochromic Potentiators of GABAA Receptors. Angew. Chem. Int. Ed. Engl. *51*: 10500–10504.

Strichartz, G.R. (1973). The inhibition of sodium currents in myelinated nerve by quaternary derivatives of lidocaine. J Gen Physiol *62*: 37–57.

Szymański, W., Beierle, J.M., Kistemaker, H.A.V., Velema, W.A., and Feringa, B.L. (2013). Reversible Photocontrol of Biological Systems by the Incorporation of Molecular Photoswitches. Chem. Rev. *113*: 6114–6178.

Tochitsky, I., Helft, Z., Meseguer, V., Fletcher, R.B., Vessey, K.A., Telias, M., et al. (2016). How Azobenzene Photoswitches Restore Visual Responses to the Blind Retina. Neuron *92*: 100–113.

Tochitsky, I., Polosukhina, A., Degtyar, V.E., Gallerani, N., Smith, C.M., Friedman, A., et al. (2014). Restoring Visual Function to Blind Mice witha Photoswitch that Exploits Electrophysiological Remodeling of Retinal Ganglion Cells. Neuron *81*: 800–813.

Velema, W.A., Szymański, W., and Feringa, B.L. (2014). Photopharmacology: Beyond Proof of Principle. J. Am. Chem. Soc. *136*: 2178–2191.

Woodhull, A.M. (1973). Ionic blockage of sodium channels in nerve. J Gen Physiol.

Yellen, G., Jurman, M.E., Abramson, T., and MacKinnon, R. (1991). Mutations affecting internal TEA blockade identify the probable pore-forming region of a K+ channel. Science *251*: 939–942.

Yizhar, O., Fenno, L.E., Davidson, T.J., Mogri, M., and Deisseroth, K. (2011). Optogenetics in Neural Systems. Neuron *71*: 9–34.
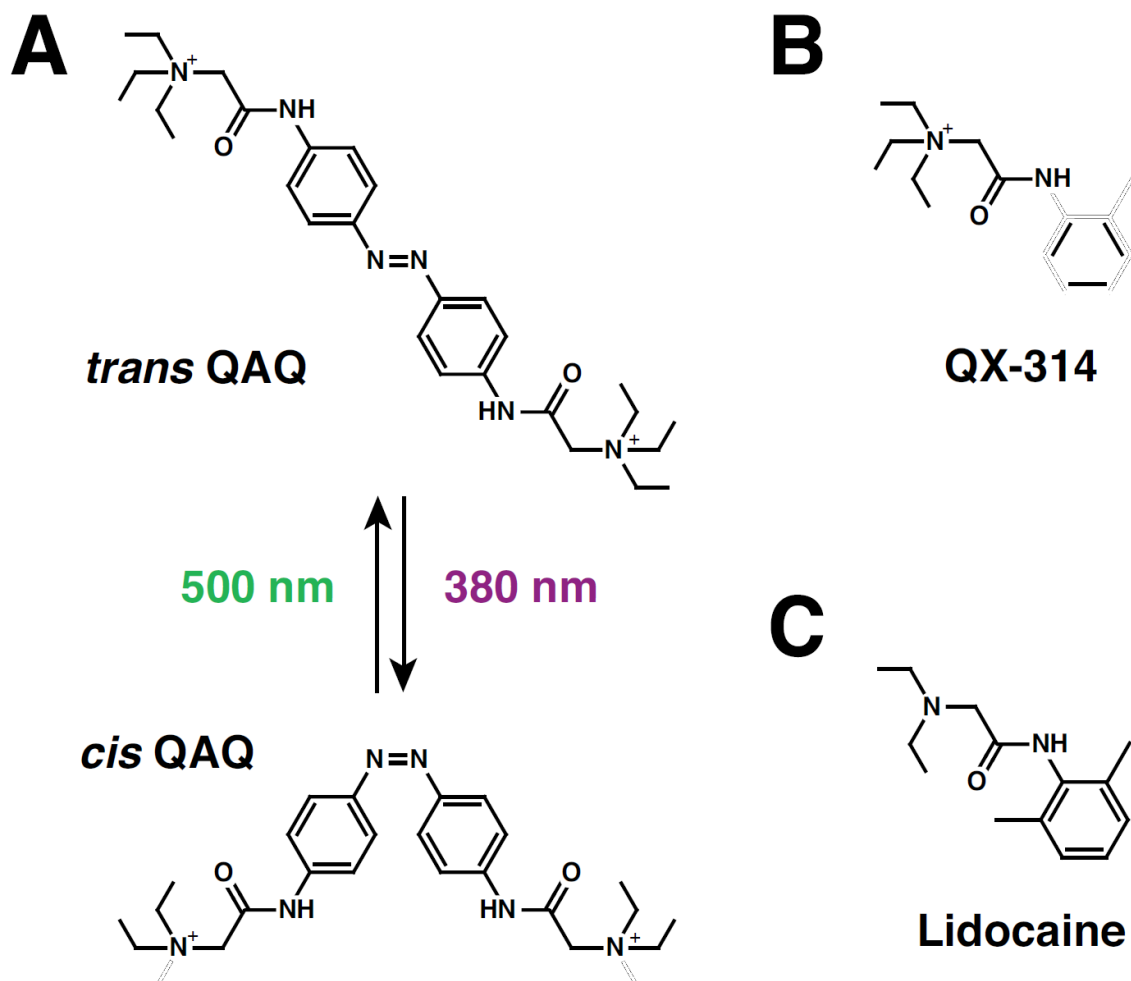
Zhou, M.M., Morais-Cabral, J.H., Mann, S.S., and MacKinnon, R. (2001). Potassium channel receptor site for the inactivation gate and quaternary amine inhibitors. Nature *411*: 657–661.

Zussy, C., Gómez-Santacana, X., Rovira, X., De Bundel, D., Ferrazzo, S., Bosch, D., et al. (2016). Dynamic modulation of in. Mol Psychiatry 1–12.
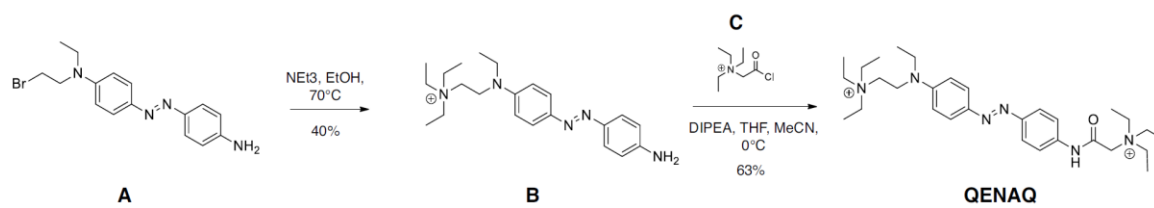
Scheme 1: Synthesis of QENAQ.

Figure 1: QAQ, a photoswitchable local anaesthetics. A) Chemical structure of *trans* and *cis* QAQ. QAQ photoisomerizes to *cis* upon illumination with near-UV light (380 nm). Isomerization back to *trans* occurs rapidly upon illumination with green light (500 nm), or slowly (min) in the dark. B) Chemical structure of QX-314. C) Chemical structure of the local anaesthetic lidocaine.
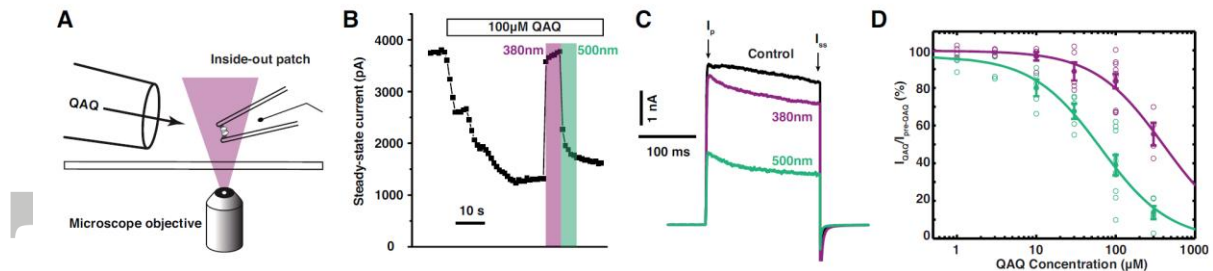
Figure 2: Concentration dependence of *cis* and *trans* QAQ blockade on Shaker-IR K$^+$ channels. A) Schematic representation of an inside-out patch recording with local perfusion tube and illumination through the microscope objective. QAQ has direct access to the internal lumen on Shaker-IR. **B)** Representative Shaker-IR current recorded at 1 Hz frequency, upon application of QAQ 100 μM, and under illumination with 380 and 500 nm light. Current was elicited by a 200 ms depolarization from -60 to +40 mV. Steady-state current (Iss), *i.e.* current at the end of the 200 ms pulse, is plotted. **C)** Representative K$^+$ current elicited by the depolarization to +40 mV, before QAQ application, and during QAQ application under green and violet light illumination. Ip: current at the peak; Iss: steady state current. **D)** Concentration dependence of QAQ block (1 Hz) under 380 nm (violet) and 500 nm light (green). IC$_{50trans}$ = 65 ± 17 μM, IC$_{50cis}$= 390 ± 111 μM (mean±95% confidence interval), open circles represent individual experiments, filled circles mean±sem, n$_{1μM}$ = 4, n$_{3μM}$ = 4, n$_{10μM}$ =5, n$_{30μM}$ =5, n$_{100μM}$ = 10, n$_{300μM}$ = 5 patches, IC$_{50}$ curve derived from data range [10, 300].
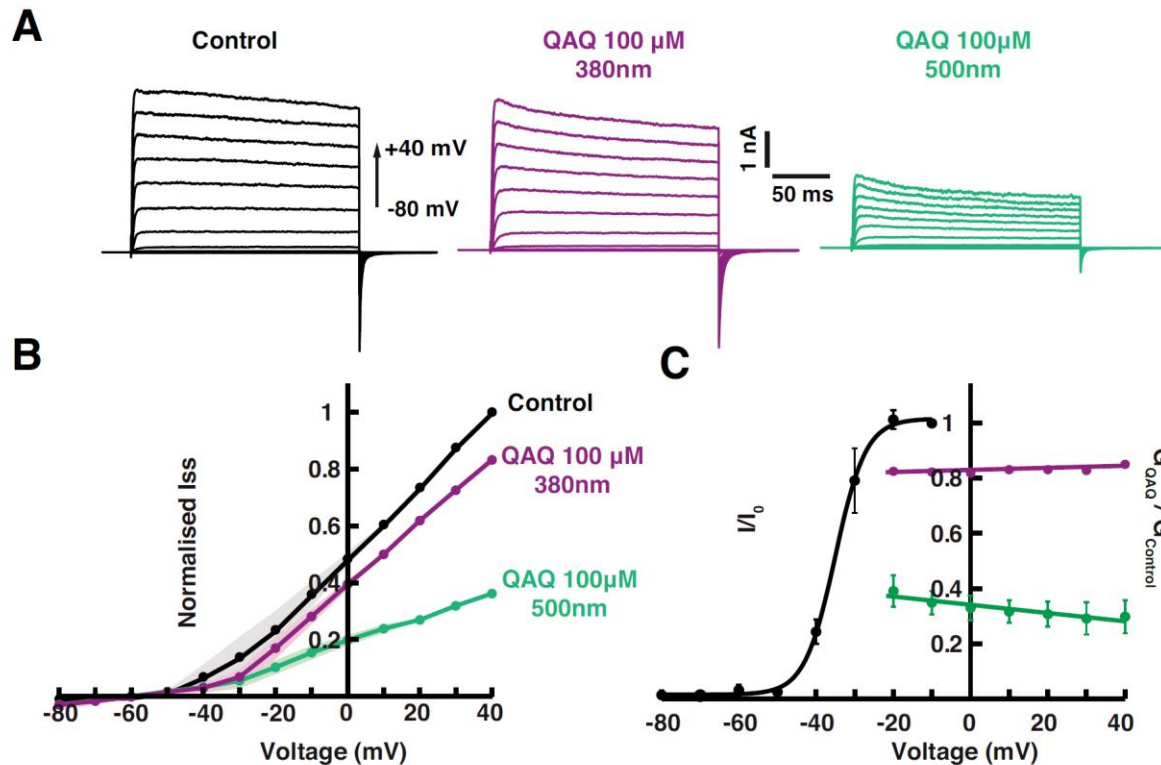
Figure 3: Voltage dependence of *cis* and *trans* QAQ blockade on Shaker-IR K$^+$ channels.
A) Representative current traces at different holding voltages (from -80 to +40 mV) before QAQ application (black), and in the presence of QAQ 100 μM under 380 (purple) or 500 nm light (green). **B)** Current-voltage relationships of Shaker-IR before QAQ application, or during QAQ application (100 μM) under 380 (purple) or 500 nm light (green). Currents were normalized to pool multiple patch recordings (n=5), solid line represents mean values, s.e.m are represented by shaded areas. **C)** Voltage dependence of *cis* (purple) and *trans* (green) QAQ blockade compared with the voltage dependence of Shaker-IR gating (black). The amplitudes of Shaker currents I are normalized (I/I$_0$) so that Iss at -10 mV is unity. The ratio of Shaker Iss current in the presence of 100 μM QAQ in either wavelength was plotted over a voltage range where Shaker-IR is fully open, i.e. for voltages >-20 mV. C*is* QAQ shows no significant voltage dependence of block (p = 0.39, Student's t test) and solid lines represents linear regression fit (m$_{cis}$ = 0.0002±0.00008 mV^{-1}). In contrast, *trans* QAQ blockade exhibited a slight voltage dependence (zδ$_{trans}$ = 0.18, K(0)$_{trans}$ = 58 μM). Error bars represent s.e.m., n=5.
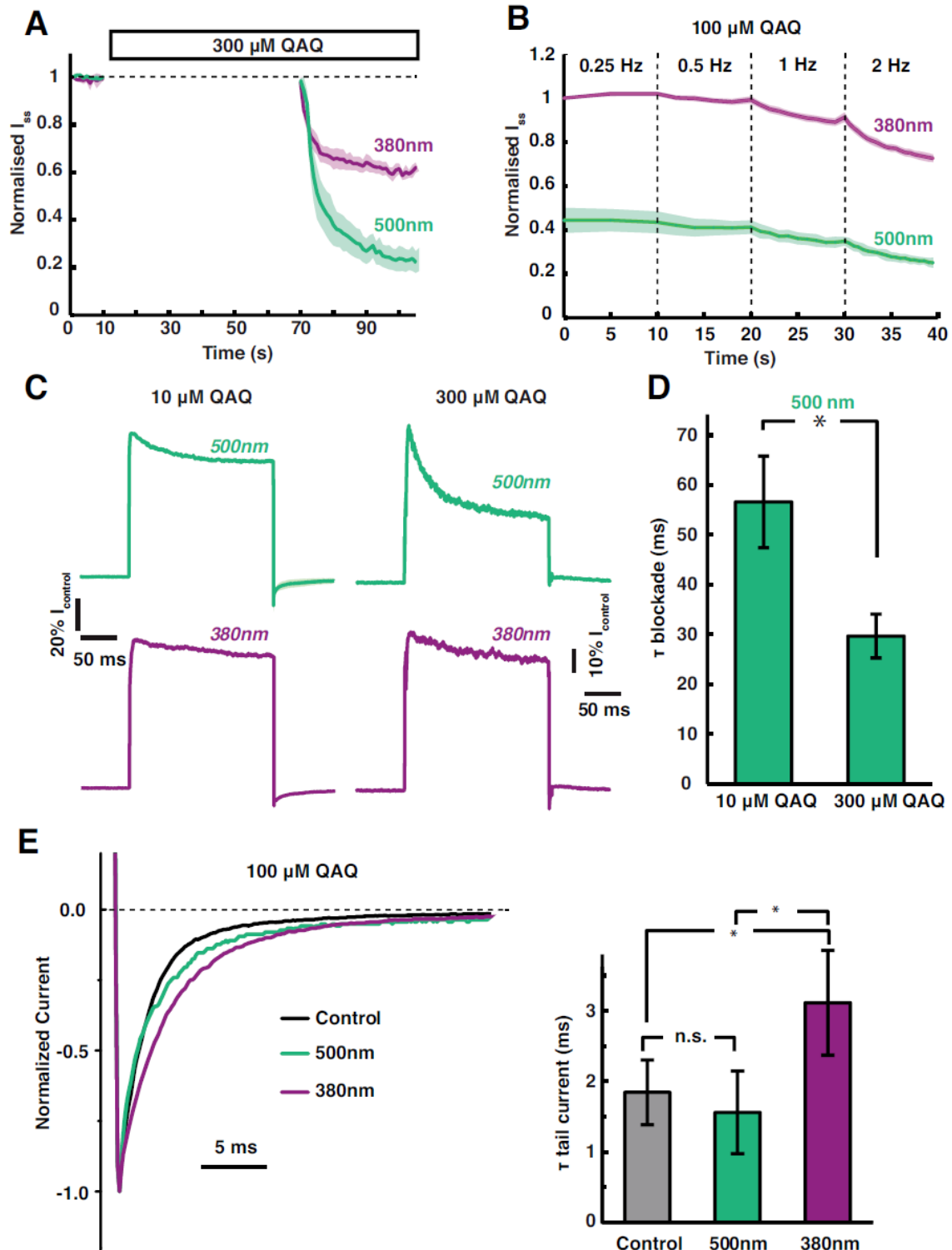
Figure 4: State-dependent interaction of QAQ with Shaker-IR. A) QAQ does not associate with closed Shaker-IR channels, neither in the *cis* nor in the *trans* form. Shaker-IR channels were kept close at negative potential (-60 mV) while QAQ was perfused either under green or under violet light. QAQ block accumulated only after channels were open using depolarization to +40 mV. Shaded areas represent s.e.m, n=4. **B)** *Cis* and *trans* QAQ are use-dependent blockers of Shaker-IR K$^+$ channels. Blockade accumulated with increased opening frequency of the channels (0.25 Hz to 2 Hz). Average of 3 examples is shown. **C)**

Representative traces for association rates of *trans* and *cis* QAQ (10 and 300 μM) to open Shaker-IR channels. Current kinetics within a 200 ms pulse (+40 mV) were normalized to control (pre-QAQ) and compared for 10 μM and 300 μM QAQ. **D)** Blockade kinetics increased with *trans* QAQ concentration (exponential fit, error bar = s.e.m., $\tau_{10\mu M} = 56.6\pm9.1$ ms, $\tau_{300\ \mu M} = 29.6\pm4.4$ ms, p=0.033, Student t-test, n=6). **E)** Closing kinetics of Shaker-IR in the absence (black) and presence of *cis* or *trans* QAQ. Representative tail currents are plotted after normalization. Inset: *Trans* QAQ ($\tau_{trans} = 1.8\pm0.5$ ms, n=6) did not affect channel closing rate ($\tau_{control} = 1.6\pm0.4$ ms, n=6, p = 0.671, Student's t test). In contrast, *cis* QAQ significantly slowed channels closing compared to *trans* QAQ ($\tau_{cis} = 3.1\pm0.7$ ms, n=6, p=0.016, Student's t-test) and also to control (p=0.047, Student's t test).
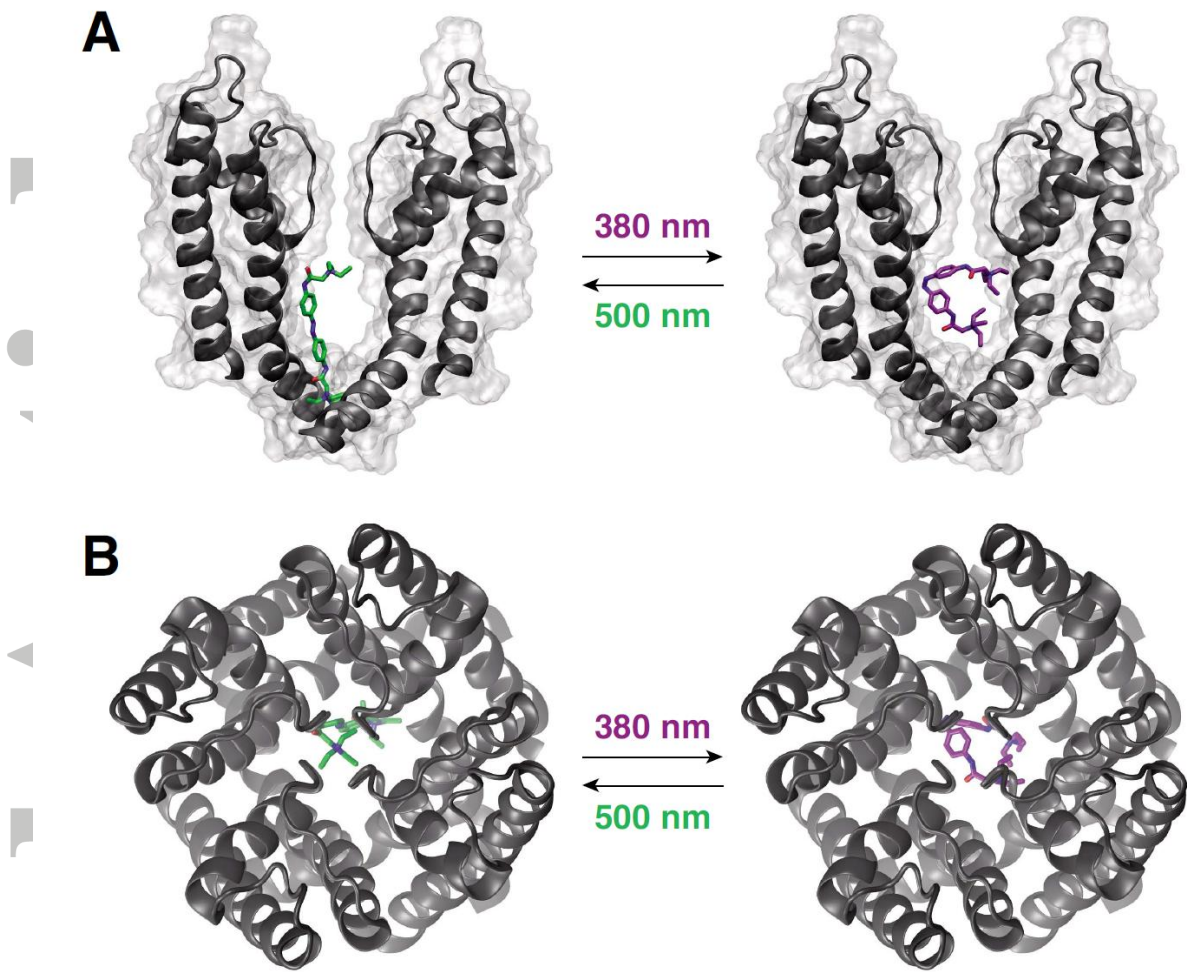
Figure 5: **Molecular docking of *cis* and *trans* QAQ to open K$^+$ channel.** Crystal structure of the open K$_V$1.2-2.1 chimera with docked QAQ isomers. The voltage-sensing domains of the K$^+$ channel are not represented, for clarity. **A)** Side view, perpendicular to the membrane. Note the position of the quaternary ammonium ion just below the selectivity filter for *trans*, but not for *cis* QAQ. Only two of the four subunits are shown, for clarity purposes. **B)** Top view, from the extracellular side.
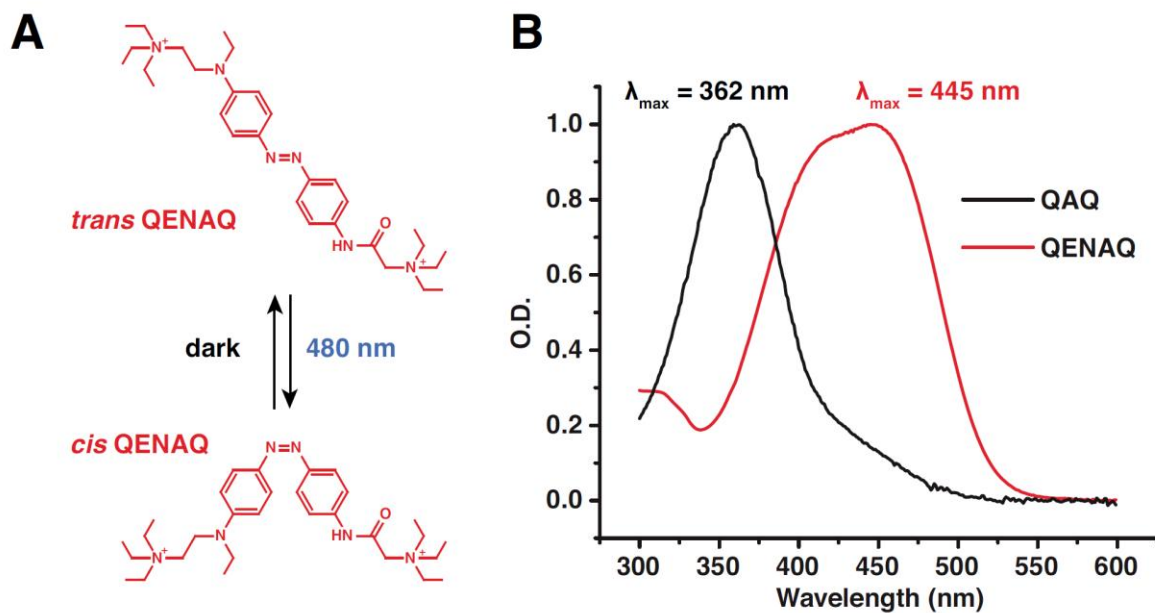
Figure 6: QENAQ, a red-shifted QAQ. A) Chemical structure of *trans* and *cis* QENAQ. QENAQ photoisomerizes to *cis* under illumination with blue light (480 nm), and reverts back to *trans* rapidly (seconds) in the dark. **B)** Absorption spectra of QAQ and QENAQ in the dark (*trans* isomer) in phosphate buffer saline, pH 7.4. $\lambda_{max} = 362$ nm for QAQ and 445 nm for QENAQ.
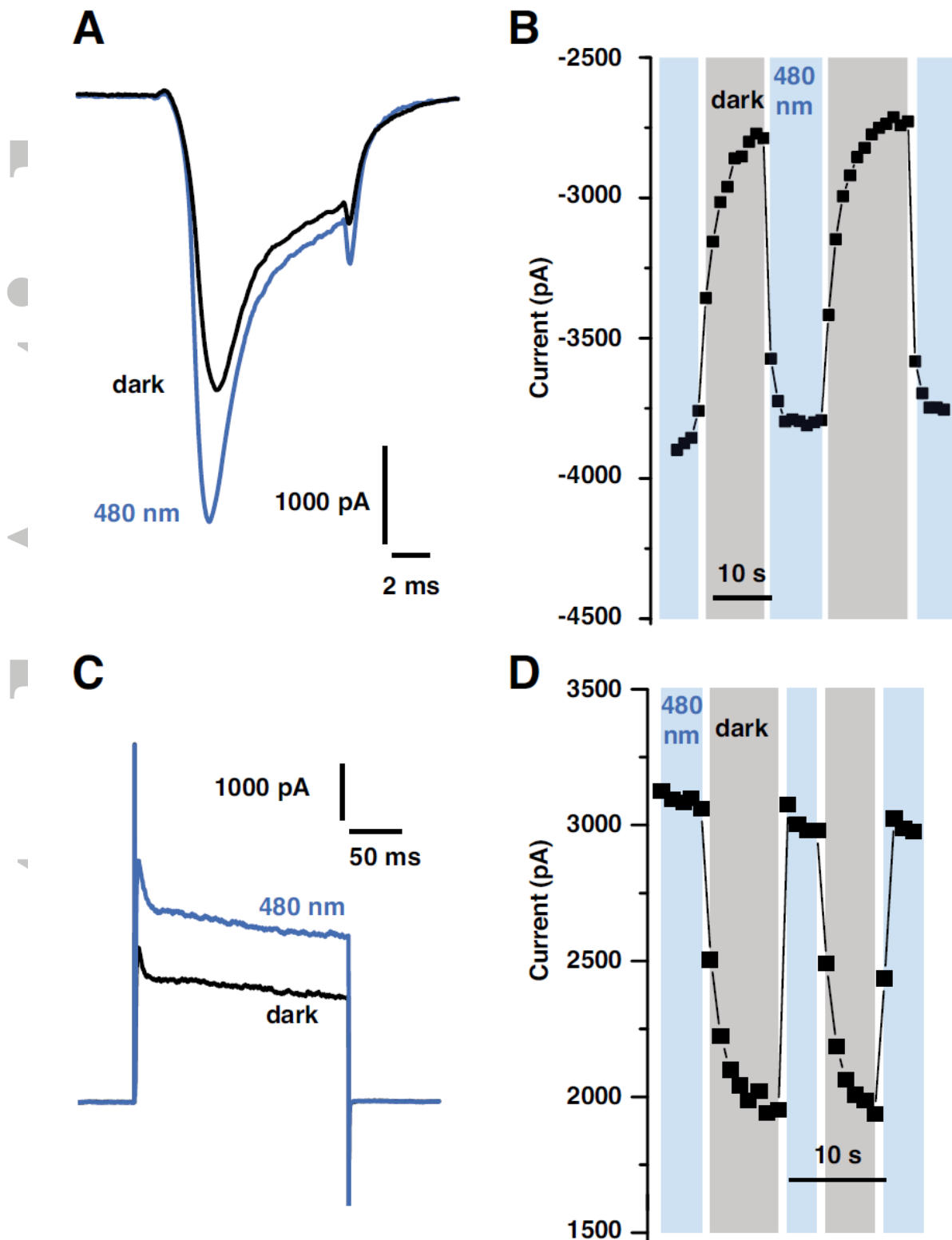
Figure 7: Optical control of native Na⁺ and K⁺ channels in dissociated trigeminal neurons with QENAQ. A) Representative voltage-gated Na^+ current from a TG neuron filled with 200 μM QENAQ, under 480 nm light and in the dark. Opening of the channels was triggered at 1 Hz using a 10 ms depolarization from -60 to -10 mV. **B)** Reversibility of Na^+ peak current photoswitching. *Cis* QENAQ was unstable in the dark and reversed to *trans* within seconds. **C)** Representative voltage-gated K^+ current from a TG neuron filled with 200

μM QENAQ, under 480 nm light and in the dark. Opening of the channels was triggered at 1 Hz using a 200 ms depolarization from -60 to +40 mV. **D)** Reversibility of K^+ steady-state current photoswitching.
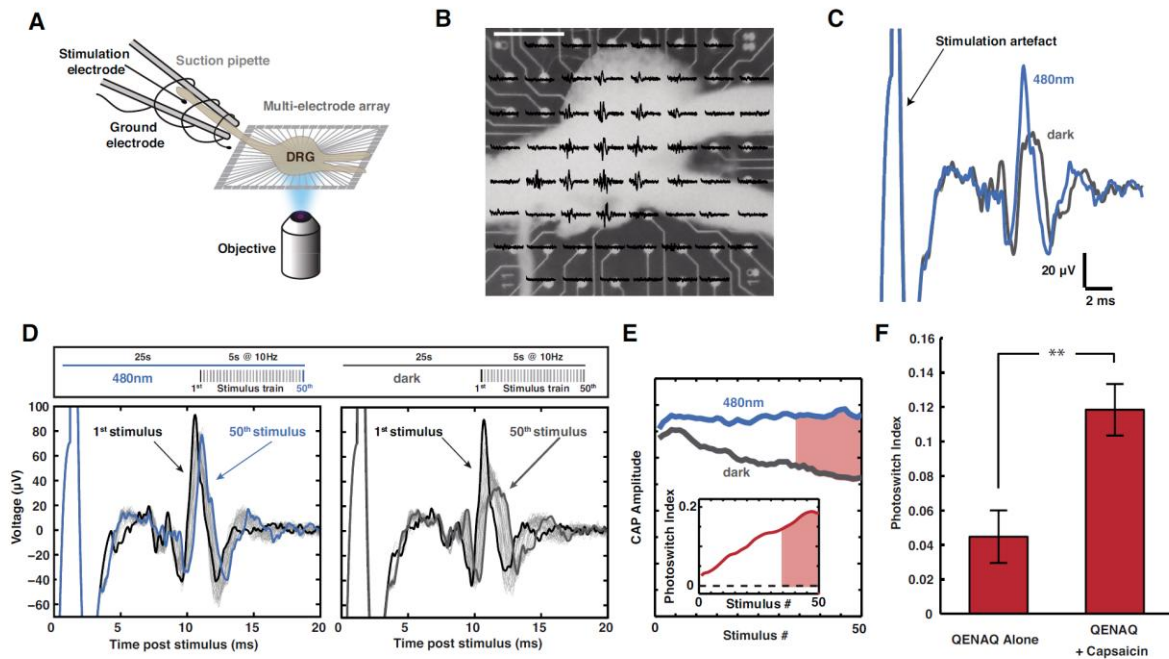
Figure 8: Optical control of intact dorsal root ganglia using visible light. A) Schematic representation of the experimental arrangement for measuring DRG photosensitization. An intact, acutely dissected mouse DRG is positioned onto an MEA with 60 electrodes. The electrodes have a three-dimensional tip shape in order to penetrate the DRG and detect signals from neurons. The peripheral nerve bundle was led into a suction electrode and electrically stimulated using a battery-driven isolator. A 4X objective was used to focus light (480 nm) onto the DRG. **B)** Image of an intact DRG mounted onto a MEA chip with superimposed nerve stimulation responses (compound action potentials, CAP). Scale bar 400 μm. **C)** CAP signals recorded from one electrode, in darkness and under 480 nm light. The DRG was pre-incubated with 300 μM QENAQ. The amplitude of evoked CAPs was smaller in darkness (*trans* QENAQ) than under illumination with blue light (*cis* QENAQ). **D)** Adaptation of CAP amplitude of a QENAQ-treated DRG under blue light and in the dark over the course of a stimulus train (5 s at 10 Hz, with 25 s pauses in between trains, upper panel). **E)** Change in CAP amplitude during a stimulus train. Because of QENAQ's use-dependence of block in darkness, the decrease in CAP amplitude accumulates over time during a stimulus train. We measured the mean CAP amplitude for each wavelength over the last 1.5 s of the stimulus train (time period shown in red) to calculate the Photoswitch Index (PI) which increases during a stimulus train (inset). **F)** The TRPV1 agonist capsaicin promotes QENAQ loading into sensory neurons. Photosensitization with QENAQ is significantly greater (p=0.0063, non-parametric ranksum test) when QENAQ is co-applied with capsaicin 1 μM (PI=0.118 ± 0.015, n=83 signals, n=6 DRGs) than alone (PI=0.045 ± 0.015, n=180 signals, n=6 DRGs).